Applied Catalysis B: Environmental 132–133 (2013) 245–255

Contents lists available at SciVerse ScienceDirect

Applied Catalysis B: Environmental

journal homepage: www.elsevier.com/locate/apcatb

Catalytic removal of formaldehyde at room temperature over supported gold catalysts

Bing-Bing Chen[a,b], Chuan Shi[a,b,*], Mark Crocker[c], Yu Wang[a,b], Ai-Min Zhu[b,**]

[a] Key Laboratory of Industrial Ecology and Environmental Engineering (MOE), Dalian University of Technology, Dalian, People's Republic of China
[b] Laboratory of Plasma Physical Chemistry, Dalian University of Technology, Dalian, People's Republic of China
[c] Center for Applied Energy Research, University of Kentucky, Lexington, KY 40511, USA

ARTICLE INFO

Article history:
Received 28 June 2012
Received in revised form 1 November 2012
Accepted 21 November 2012
Available online 3 December 2012

Keywords:
Formaldehyde
Catalytic oxidation
Au/CeO_2
Room temperature

ABSTRACT

Two kinds of Au/CeO_2, prepared by deposition–precipitation (DP) using urea (U) or NaOH (N) as precipitants were investigated as catalysts for HCHO oxidation. H_2-TPR and XPS techniques were used to characterize the Au/CeO_2 samples. Due to the generation of increased amounts of active surface oxygen species resulting from the strong Au–CeO_2 interaction, the Au/CeO_2 (DPU) catalyst showed higher activity than the DPN catalyst, achieving 100% conversion of HCHO into CO_2 and H_2O at room temperature, even in the presence of water and at high GHSV (143,000 h^{-1}); moreover, the conversion was stable for at least 60 h. The reaction mechanism and the rate limiting steps for HCHO oxidation over the Au/CeO_2 catalysts were identified by means of *in situ* DRIFTS studies. The influence of oxygen and water on the formation and consumption of the formate reaction intermediates was also investigated. Results suggest that Au/CeO_2 (DPU) is a promising catalyst for HCHO removal under real world conditions.

© 2012 Elsevier B.V. All rights reserved.

1. Introduction

Formaldehyde is one of the most common and most noxious indoor gaseous pollutants. It is commonly emitted from materials used for the construction of buildings, as well as from decorative materials. Long-term exposure to indoor air containing HCHO, even at the ppm level, may cause adverse effects on human health [1]. Significant efforts have been made to remove low concentrations of HCHO from indoor air. There are generally two methods that can be considered from both practical and economic points of view, one being conventional physical adsorption and/or chemical reaction. The other is catalytic oxidation. Conventional physical adsorption and/or chemical reaction using impregnated potassium permanganate or organic amines is efficient for HCHO elimination, but these adsorbents are effective for only a short period due to their limited removal capacities [2,3]. In contrast, catalytic oxidation has great potential for the continuous degradation of HCHO, which yields CO_2 and H_2O as the final products.

Catalysts applied for HCHO oxidation include both supported base metals and noble metals. However, base metals require the use of elevated temperatures for HCHO oxidation. For example, the operating temperature of MoO_3–SnO_2, MnO_x–CeO_2 and Ag/CeO_2 catalysts is in the range of 100–300 °C [4–9]. In contrast, noble metal catalysts such as Ru, Pd and Pt can effectively remove HCHO at low temperature [10–15]. Among them, supported Pt catalysts have been proven to be the most active. He et al. [12], Leung et al. [13], Jia et al. [14], and Shen et al. [15] reported that HCHO could be completely oxidized into CO_2 and H_2O at room temperature over 1 wt% Pt/TiO_2, 0.1 wt% Pt–TiO_2, 1 wt% Pt/Fe_2O_3 and 3 wt% Pt/MnO_x–CeO_2, respectively.

Formerly, gold was believed to be poorly active as a heterogeneous catalyst due to its electronic configuration. However, in 1989 Haruta et al. discovered that supported, highly dispersed particles of metallic gold exhibit remarkable activity for CO oxidation at low temperature [16]. This finding has initiated significant interest in gold catalysis. Apart from low temperature CO oxidation, gold catalysts have been proved to be active in many other catalytic reactions, such as the hydrogenation of carbon oxides, the water–gas shift reaction and the oxidation of volatile organic compounds (VOCs) [17–22]. Fe_2O_3-, ZrO_2- and CeO_2-supported Au catalysts have been found to be active for formaldehyde oxidation [23–25], although the temperature required for total conversion of formaldehyde is in excess of 100 °C [26]. In addition, ordered forms of CeO_2 such as three-dimensional ordered macroporous (3DOM) ceria have been explored as supports for Au catalysts and have been shown to be more active than samples lacking long range order and high surface, due to the uniform macroporous structures and high surface leading to good distribution of catalytic species of

* Corresponding author at: Key Laboratory of Industrial Ecology and Environmental Engineering (MOE), Dalian University of Technology, Dalian, People's Republic of China. Tel.: +86 411 84986083.
** Corresponding author at: Laboratory of Plasma Physical Chemistry, Dalian University of Technology, Dalian, People's Republic of China. Tel.: +86 411 84706094.
E-mail addresses: chuanshi@dlut.edu.cn (C. Shi), amzhu@dlut.edu.cn (A.-M. Zhu).

0926-3373/$ – see front matter © 2012 Elsevier B.V. All rights reserved.
http://dx.doi.org/10.1016/j.apcatb.2012.11.028

Au [27,28]. For example, Au supported on 3DOM CeO_2, as well as the high surface area Au/CeO_2 prepared by Lu et al., is reported to completely oxidize HCHO at 75 °C and 50 °C, respectively [27,29]. Though there are reports on removal of HCHO at room temperature over Au/TiO_2 catalyst [30], the high activity of Au/CeO_2 catalysts for removal of HCHO at room temperature has never been reported in the published literatures.

Herein, Au/CeO_2 catalysts prepared by deposition–precipitation (DP) with different precipitants were tested for catalytic HCHO oxidation. Structural analysis of the catalysts was performed and subsequently correlated with their catalytic performance to investigate the origin of high HCHO oxidation activity. It was found that the catalyst prepared by DP using urea as precipitant showed the best catalytic activity, complete oxidation of HCHO into CO_2 and H_2O being achieved at room temperature, even in wet air. Using *in situ* DRIFTS measurements, the intermediates formed during HCHO oxidation were identified.

2. Experimental

2.1. Catalyst preparation

Au/CeO_2 catalysts with nominal gold loading of 1 wt% were prepared by the deposition–precipitation method, using either urea or NaOH as precipitant. In the case of the DP method with urea [24], an aqueous solution of $HAuCl_4$ (22 mL, 10 g L^{-1}) was first mixed with 10.0 g of CeO_2 and then diluted with 400 mL of deionized (D.I.) water. Subsequently, a designated amount of urea in a molar ratio of gold to urea of 1/125 was added as the precipitating agent. The mixture was stirred at 80 °C for 8 h and then aged for 12 h at room temperature, after which the mixture was filtered to separate the solid from the liquid. The solid product was washed three times with D.I. water, dried in air at 80 °C for 16 h, and calcined in air at 200 °C for 4 h.

In the case of the DP method with NaOH [29], an aqueous solution of $HAuCl_4$ (4 mL, 10 g L^{-1}) was heated to 70 °C and brought to pH ≈ 7 by the addition of 0.1 M NaOH solution, after which 2.0 g of CeO_2 was added. After adjusting the suspension to pH ≈ 7, it was vigorously stirred at 70 °C for 1 h. The solid was then isolated by centrifugation and washed until free of chloride and dried at 70 °C for 3 h. Next, the catalyst was calcined at 200 °C for 4 h. Samples are coded as follows: Au/CeO_2 (DPU) for the catalyst prepared by deposition–precipitation with urea, Au/CeO_2 (DPN) for the catalyst prepared by deposition–precipitation with NaOH.

2.2. Catalyst characterization

The actual Au content in the catalyst was determined by inductively coupled plasma-atomic emission spectroscopy (ICP-AES, Optima 2000DV, USA).

High-resolution transmission electron microscopy (HRTEM) micrographs were obtained with a Tecnai G2 20 S-TWIN microscope and operated at 200 kV.

Hydrogen temperature programmed reduction (H_2-TPR) measurements were performed in a fixed bed microreactor, equipped with a TCD detector. 50 mg samples were loaded and pretreated under Ar at 100 °C for 1 h to remove adsorbed CO_2 and H_2O. After cooling to 30 °C and then introducing the reducing gas (5% H_2/Ar) at a flow rate of 50 mL min^{-1}, the temperature was ramped to 300 °C at 10 °C min^{-1}.

The surface chemical states of the Au/CeO_2 catalysts were examined by X-ray photoelectron spectroscopy (XPS, ESCALAB250 Thermo VG, USA) using an Al Kα X-ray source (1486.6 eV) operated at 15 kV and 300 W. The reference energy used for calibration was the C 1s signal at 284.6 eV.

Infrared spectra were recorded on a Bruker Tensor 27 instrument equipped with a MCT detector using the DRIFT technique. Scans were collected from 4000 to 1100 cm^{-1} (128 scans, resolution of 4 cm^{-1}). In adsorption experiments, the catalyst was placed in a DRIFT cell equipped with CaF_2 windows and was pretreated in a N_2 flow at 200 °C for 1 h. Subsequently, the reactant gas mixture (80 ppm HCHO/21% O_2/H_2O (RH = 50%)/N_2) was introduced into the DRIFT cell at room temperature *via* separate mass flow controllers at a flow rate of 100 mL min^{-1}. After a specified amount of time the HCHO flow was switched off and replaced by wet air (RH = 50%).

2.3. Catalytic activity measurement

Catalyst tests were performed in a continuous flow fixed-bed quartz microreactor at atmospheric pressure. 0.25 g catalyst (0.176 mL, 40–60 mesh) was sandwiched between quartz wool layers in the tube reactor. All the feed gases used in this work were of high-purity grade (99.99%). The gas flow rates were adjusted and controlled by mass flow controllers. Gaseous HCHO was generated by flowing N_2 over paraformaldehyde (99%, Aldrich) in a thermostated bath. The concentration of HCHO was controlled by adjusting the flow rate of N_2 and the temperature of the thermostated bath. Gaseous H_2O was carried into the gas stream by passing N_2 through a bubbler in a water bath at room temperature. The amount of water, expressed as the relative humidity (RH) at 25 °C, was controlled by adjusting the flow rate of N_2, while keeping the total flow unchanged. The HCHO/N_2 and H_2O/N_2 streams were then mixed with the main gas stream of O_2/N_2, leading to a typical feed gas composition of 80 ppm HCHO and 21 vol.% oxygen, balanced by nitrogen with a relative humidity (RH) of 50%. The total flow rate was 100 mL min^{-1}, corresponding to a gas hourly space velocity (GHSV) of 34,000 h^{-1}.

Concentrations of CO and CO_2 were measured online using an infrared absorption spectrometer (SICK-MAIHAK-S710, Germany). In this work, it was not possible to monitor the HCHO concentration directly by Fourier transform-infrared spectroscopy (FT-IR) due to the interfering effects of water. Therefore, HCHO was measured by converting it to CO_2 in a homemade HCHO-to-CO_2 converter ($CuO–MnO_2/\gamma$-Al_2O_3 catalyst) at 300 °C and determining the amount of CO_2 formed. Several previous reports have likewise pointed out that for the accurate determination of HCHO, the HCHO should first be oxidized to CO_2 [31,32].

Conversion of HCHO was calculated as follows:

$$\text{HCHO conversion}\,(\%) = \frac{[CO_2]_{out}\text{vol.}\%}{[HCHO]_{in}\text{vol.}\%} \times 100,$$

where $[CO_2]_{out}$ is the concentration in the products (vol.%) and $[HCHO]_{in}$ is the HCHO concentration in the feed gas (vol.%). In all cases the carbon balance was near 100% [29].

3. Results

3.1. Physicochemical properties of the catalysts

The ICP results show that the two samples have a similar Au content of *ca.* 0.8%. The Au/CeO_2 sample prepared using urea as precipitant (0.83%) has a slightly higher Au content than the one prepared using NaOH as precipitant (0.78%).

The morphology and structure of the Au-NPs were determined from high-resolution transmission electron micrographs (HRTEM) and the images were shown in Fig. 1. The identification of Au and CeO_2 was evidenced by *d*-spacing measurements. The Au-NPs were spherical and the Au (2 0 0) plane and Au (1 1 1) plane were observed in the HRTEM images of Au/CeO_2 (DPU) and Au/CeO_2 (DPN) catalysts, respectively. The mean particle size of Au-NPs was determined to be in the range of 2–4 nm in the Au/CeO_2 (DPU)

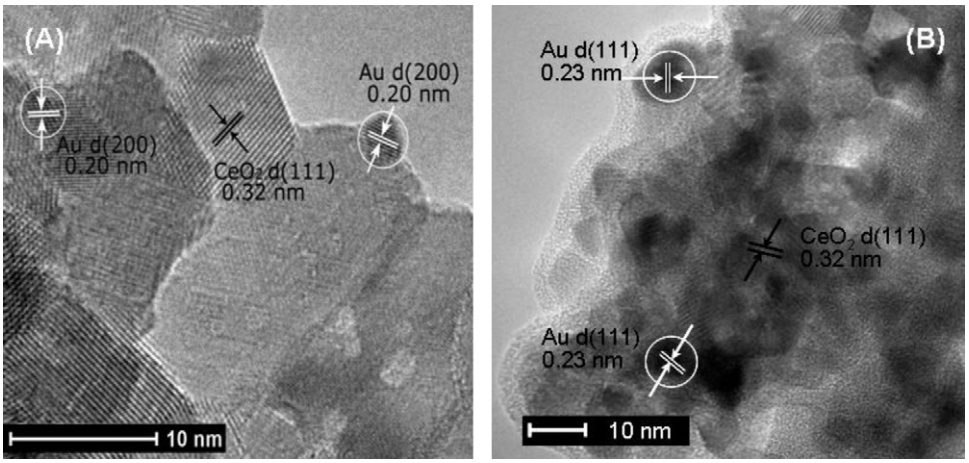

Fig. 1. HRTEM images of Au/CeO_2 catalysts. (A) Au/CeO_2 (DPU); (B) Au/CeO_2 (DPN).

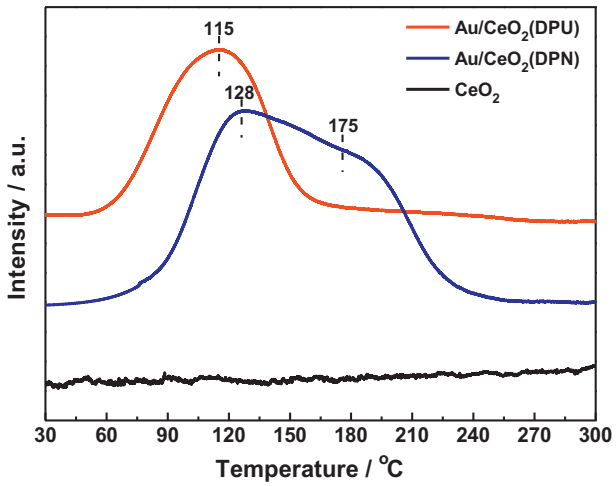

Fig. 2. H_2-TPR profiles of 1 wt% Au/CeO_2 (DPU) and 1 wt% Au/CeO_2 (DPN) catalysts.

catalyst and those were larger in the Au/CeO_2 (DPN) (8–10 nm) catalyst (an average obtained from the measurement of 100 Au-NPs), which indicating that the type of precipitants would have effect on the Au size distribution in the sample.

The H_2-TPR profiles of the Au/CeO_2 catalysts are presented in Fig. 2. In the temperature range examined (30–300 °C), pure CeO_2 showed no reduction peak [33]. In comparison, for the Au/CeO_2 samples the peak related to the reduction of ceria surface oxygen shifted to lower temperatures. For the Au/CeO_2 (DPN) catalyst, the one broad reduction peak with a maximum at 128 °C was observed, followed by another reduction maximum at 175 °C. In contrast, the Au/CeO_2 (DPU) catalyst showed only one reduction peak at the even lower temperature of 115 °C. Evidently, the surface oxygen species on the Au/CeO_2 (DPU) catalyst are more easily reduced than those on the Au/CeO_2 (DPN) catalyst, *i.e.*, the active oxygen species formed on the Au/CeO_2 (DPU) sample are more reactive. The fact that reduction events shifted to lower temperatures over the Au-loaded ceria samples compared with the bare support indicates that the presence of gold facilitates the reduction of surface oxygen species. It has been suggested that this might be due to weakening of the surface Ce—O bond caused by the presence of Au [34,35].

XPS measurements were conducted on the Au-loaded samples, the results being shown in Fig. 3. The Au 4f core level spectra of the catalyst could be deconvoluted into several components and the results are listed in Table 1. The typical binding energies of Au $4f_{7/2}$ at 84.0 eV and 85.6 eV are assigned to Au^0 and Au^{3+}, respectively, suggesting that there are two valence states in the Au/CeO_2 (DPU) catalyst corresponding to ionic Au^{3+} and metallic Au^0 [21,36]. In the case of the Au/CeO_2 (DPN) catalyst, the same Au valence states were observed. Additionally, a signal corresponding to Au^{1+} was observed (binding energy of Au $4f_{7/2}$ at 84.5 eV), implying that Au^0, Au^{1+} and Au^{3+} were present in the Au/CeO_2 (DPN) catalyst. Based on the deconvolution results, the ratio of Au^{3+} to total surface Au was calculated, as shown in Table 1. From this, it is clear that the amount of Au^{3+} species in the DPU sample is at least three times higher than that in the DPN sample, indicating that the use of different precipitants during catalyst preparation results in very different distributions of the Au species.

To provide further insights into the surface chemical state of Au and the correlation between Au and Ce states, the Ce 3d core level of the catalyst was also examined, the deconvolution results being shown in Table 1, where V and U indicate the spin-orbit coupling $3d_{5/2}$ and $3d_{3/2}$, respectively. The Ce $3d_{5/2}$ peaks marked as v (883.4 eV), v″ (890.1 eV) and v‴ (899.9 eV) correspond to the Ce^{4+} state, whereas that denoted as v′ at 885.5 eV is assigned to Ce^{3+}, implying that Ce is present in the mixed valence state in the Au/CeO_2 (DPU) catalyst [37,38]. The same Ce valence states were observed in the Au/CeO_2 (DPN) catalyst, although the proportion of surface Ce^{3+} species in the catalysts was different, as shown in Table 1. Specifically, it is observed that the ratio of Ce^{3+} in the DPU catalyst is higher than that in the DPN catalyst. Combining this result with the finding that the relative amount of Au^{3+} in the DPU sample is also higher than in the DPN sample, it is proposed that there is charge transfer from Au to Ce, resulting in a higher relative concentration of Au^{3+} accompanied by an increased concentration of Ce^{3+} in the Au/CeO_2 (DPU) sample [39–41].

Table 1
XPS analysis of Au/CeO_2 catalysts.

Catalyst	Peak position (eV)			$Au^{3+}/Au^0 + Au^+ + Au^{3+}$ (at.%)	$Ce^{3+}/Ce^{3+} + Ce^{4+}$ (at.%)
	Au^0	Au^+	Au^{3+}		
Au/CeO_2(DPN)	84.0	84.5	85.6	21.8	14.9
Au/CeO_2(DPU)	84.0	–	85.6	79.9	22.8

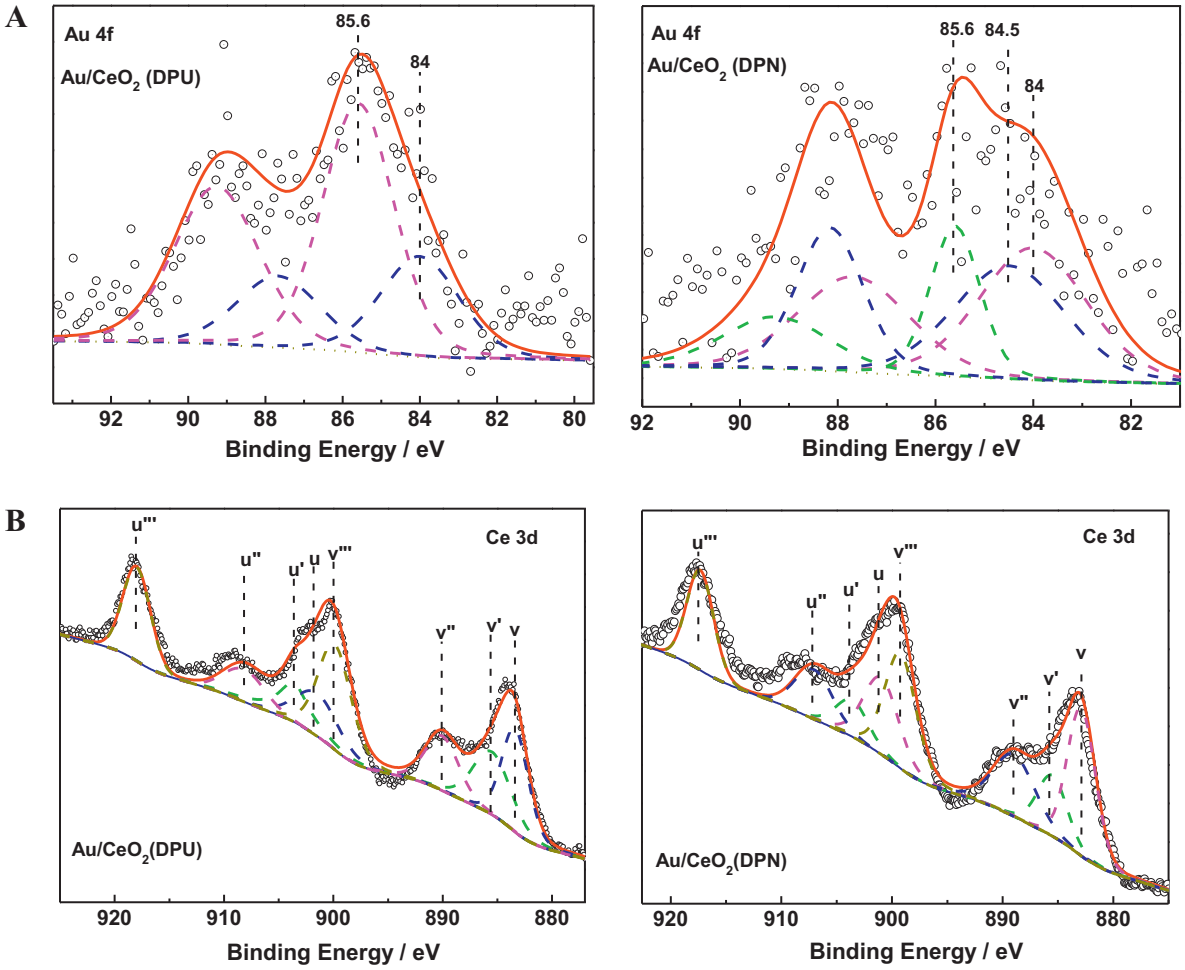

Fig. 3. (A) Au 4f XPS spectra of Au/CeO_2 (DPU) and Au/CeO_2 (DPN) catalysts. (B) Ce 3d XPS of Au/CeO_2 (DPU) and Au/CeO_2 (DPN) catalysts.

3.2. Catalytic activity

The catalytic activities of the Au/CeO_2 catalysts were evaluated in HCHO oxidation, the results being collected in Fig. 4. It can be seen that the Au/CeO_2 (DPN) catalyst showed the lower conversion at room temperature, complete HCHO conversion being obtained at 70 °C. In contrast, HCHO could be completely oxidized over Au/CeO_2 (DPU) at room temperature; indeed, it appears to be among the most active catalysts reported in the literature [11,12,15,25,27–29,42–48].

Fig. 5 shows the effect of humidity on catalyst performance. In both dry and wet air, 100% conversion was achieved, which suggests that the presence of water did not significantly inhibit the

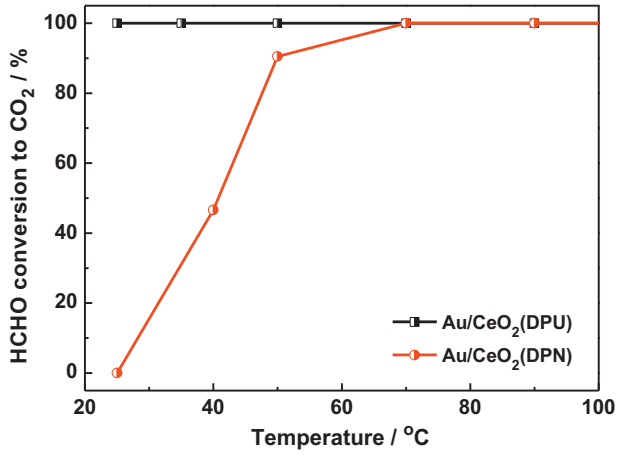

Fig. 4. Catalytic oxidation of HCHO over 1 wt% Au/CeO_2 (DPU) and 1 wt% Au/CeO_2 (DPN) catalysts. Reaction conditions: 80 ppm HCHO/21%O_2/N_2, RH = 50% (25 °C); temperature: 25 °C; GHSV = 34,000 h^{-1}.

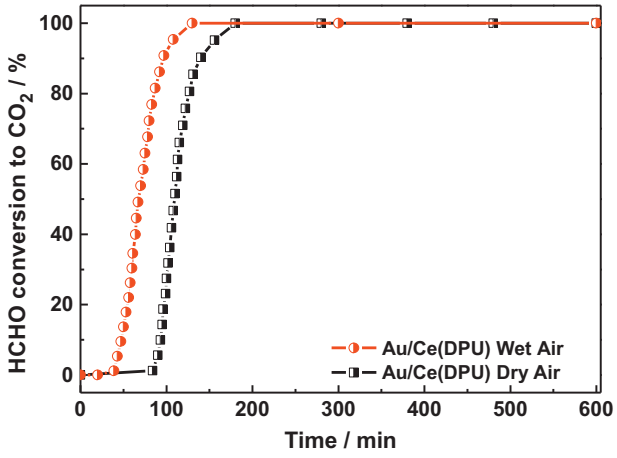

Fig. 5. Effect of water on HCHO conversion over the 1 wt% Au/CeO_2 (DPU) catalyst. Reaction conditions: wet air: 80 ppm HCHO/21%O_2/N_2, RH = 50% (25 °C); temperature: 25 °C; GHSV = 34,000 h^{-1}; dry air: 80 ppm HCHO/21%O_2/N_2; temperature: 25 °C; GHSV = 34,000 h^{-1}.

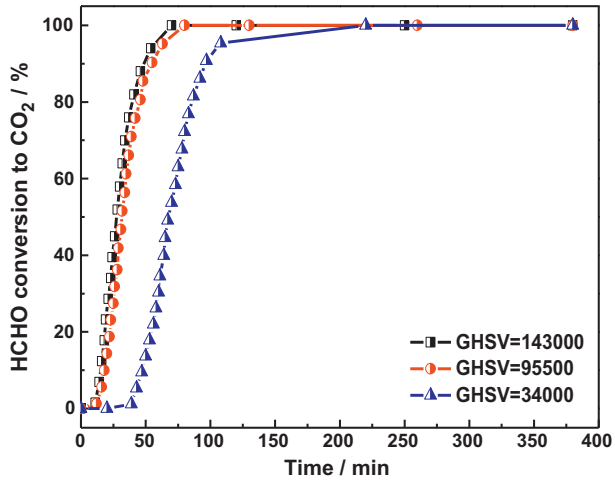

Fig. 6. Effect of GHSV on HCHO conversion over 1 wt% Au/CeO_2 (DPU). Reaction condition: 80 ppm HCHO/21%O_2/N_2, RH = 50%; temperature: 25 °C.

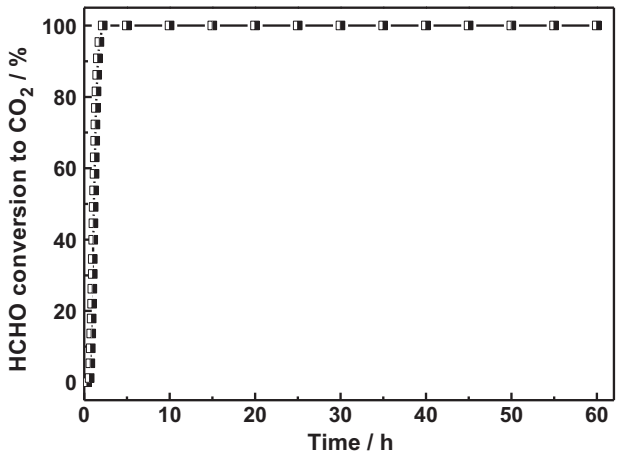

Fig. 7. Durability test using 1 wt% Au/CeO_2 (DPU) catalyst. Reaction conditions: 80 ppm HCHO/21%O_2/N_2, 50%RH; temperature: 25 °C; GHSV = 34,000 h^{-1}.

activity of the catalyst [42]. It is interesting that the oxidation of HCHO shows a distinct induction period over the catalyst in both dry and wet air, although the induction period under wet conditions was shorter.

The effect of GHSV on HCHO conversion at ambient temperature was studied by fixing the initial HCHO concentration at 80 ppm and relative humidity at 50%. Fig. 6 compares the conversions of HCHO over the 1% Au/CeO_2 (DPU) catalyst at different GHSV. The steady state conversion of HCHO was 100% at 34,000 h^{-1}, 95,500 h^{-1} and 143,000 h^{-1}, *i.e.*, the conversion remained unchanged, although the induction period shortened with increasing GHSV. The fact that the 1% Au/CeO_2 (DPU) catalyst exhibited total HCHO conversion to CO_2 even at the extremely high GHSV of 143,000 h^{-1} suggests that it is a promising catalyst for practical indoor HCHO removal.

A durability test on the 1% Au/CeO_2 (DPU) catalyst was conducted under conditions corresponding to 80 ppm initial HCHO concentration, 50% relative humidity, and 34,000 h^{-1} GHSV. As shown in Fig. 7, complete conversion of HCHO was achieved and no deactivation could be observed after operation for 60 h, indicating that the 1% Au/CeO_2 (DPU) catalyst is quite stable under these conditions.

3.3. *In situ* DRIFTS study of reaction mechanism

3.3.1. Formation of reaction intermediates

In situ DRIFT spectra of the Au/CeO_2 (DPN) catalyst obtained upon exposure to different gas streams at room temperature are shown in Fig. 8. The bands assignments to formaldehyde, formate, dioxymethylene and water species in the literatures were summarized in Table 2. Upon exposure to 80 ppm HCHO/N_2, bands were observed at 1575, 1375 and 1358 cm^{-1} (Fig. 8A). According to the literature, the band at 1575 cm^{-1} is due to the asymmetric ν_{as}(COO) stretch of formate species and the bands at 1375 and 1358 cm^{-1} are due to the corresponding symmetric ν_s(COO) stretch [29,49]. No peaks associated with formaldehyde were detected, consistent with immediate oxidation of the HCHO after its adsorption. Upon introducing O_2 into the HCHO-containing feed stream, similar bands attributed to formate species were observed and the relative intensity of these bands appeared unchanged, as shown in Fig. 8B. Upon exposure to 80 ppm HCHO/H_2O (RH = 50%)/N_2, a band at 1648 cm^{-1} due to adsorbed water δ(H-O-H) and a band at 3420 cm^{-1} due to isolated hydroxyl groups ν(OH) strongly perturbed by hydrogen bonding appeared, while the intensities of the formate bands became relatively stronger [49,50]. This result implies that the presence of water accelerated the formation of the formate species. Finally, the spectra resulting from exposure to 80 ppm HCHO/21%O_2/H_2O (RH = 50%)/N_2 were nearly the same as the above case, bands attributed to formate species and adsorbed water being observed. These observations suggest that formate species were the main intermediates of HCHO oxidation over the Au/CeO_2 (DPN) catalyst at room temperature.

In the case of the Au/CeO_2 (DPU) sample, results were somewhat different as shown in Fig. 9. Upon exposure to 80 ppm HCHO/N_2, the

Table 2A
Observed wave numbers (cm^{-1}) of adsorbed formaldehyde and formate in the literatures [7,49–51].

HCHO				Formate		
Ass.	Gas [52]	On TiO_2	On Al_2O_3	Ass.	On TiO_2	On CeO_2
$\upsilon_s(CH_2)$	2783		2818	υ(CH)	2885	2845 2832
υ(CO)	1746	1710	1718	υ_{as}(COO)	1575, 1560, 1557	1599, 1568, 1556, 1542
$\delta(CH_2)$	1500		1498	υ_s(COO)	1370, 1340	1376, 1362, 1359

Table 2B
Observed wave numbers (cm^{-1}) of adsorbed dioxymethylene and water in the literatures [7,49,50].

DOM			Water	
Ass.	On TiO_2	On CeO_2	Ass.	On TiO_2 and CeO_2
$\omega(CH_2)$	1418–1408	1415	υ(OH)	3600–3050
$\gamma(CH_2)$	1186, 1138	1130, 1076	δ(OH)	1648, 1624
	1114, 1086	964, 924	Ad H_2O	1620
υ(CO)	858			

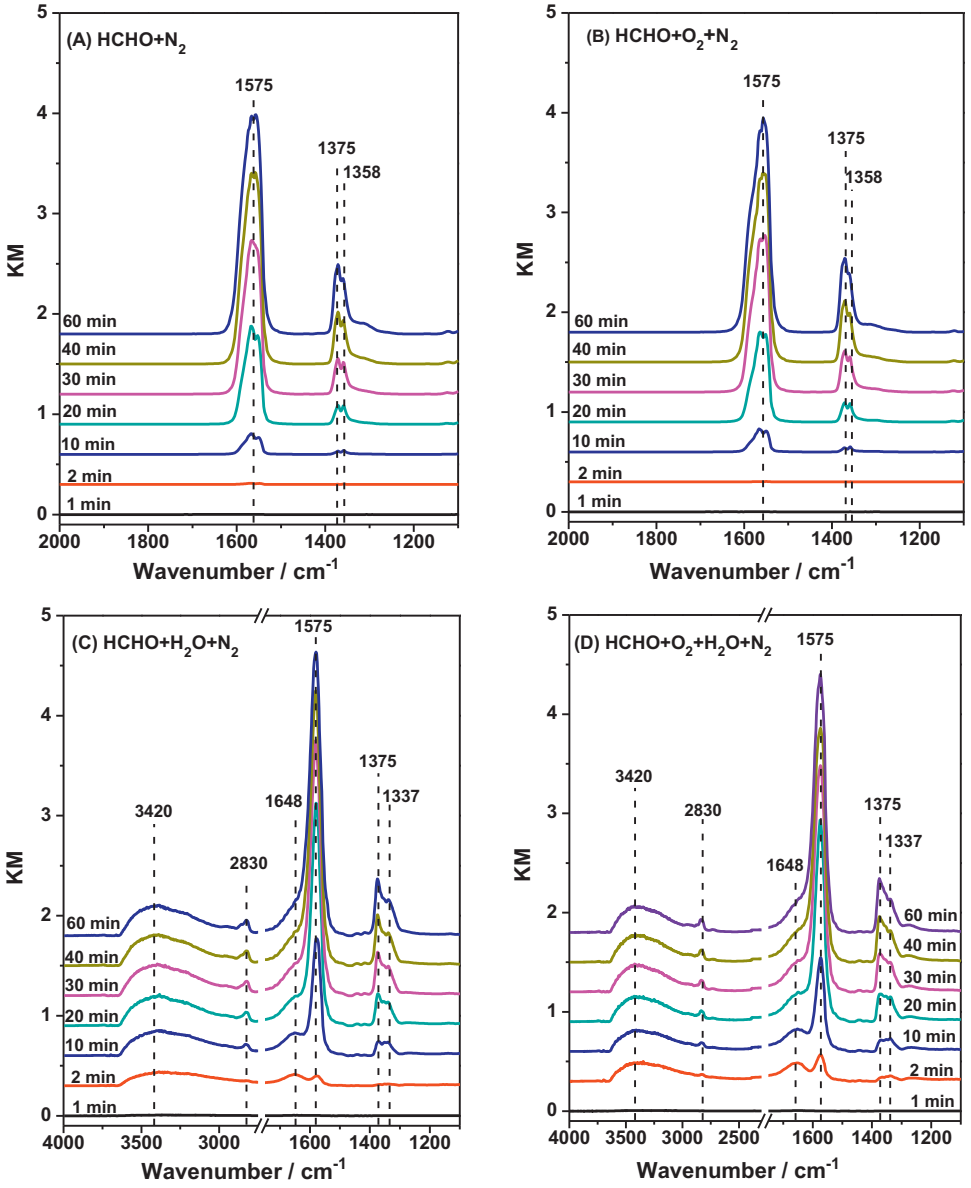

Fig. 8. *In situ* DRIFT spectra of HCHO adsorption on 1 wt% Au/CeO_2 (DPN) in different atmospheres at RT.

same characteristic bands at 1575, 1372 and 1358 cm^{-1} ascribed to formate species were detected. With increasing time, the intensity of the bands increased, indicating that the HCHO was rapidly oxidized to formate by the surface oxygen of the Au/CeO_2 (DPU) catalyst. In the presence of 21% O_2, the bands ascribed to formate species were also observed (Fig. 9B). Upon exposure to the 80 ppm $HCHO/H_2O$ (RH = 50%)/N_2, the band at 1648 cm^{-1} due to adsorbed water δ(H-O-H) and the band at 3420 cm^{-1} due to hydroxyl groups ν(OH) appeared, while a band ascribed to dioxymethylene (DOM, 1442 cm^{-1}) was also observed, which is due to the partial oxidation of HCHO and it could further combine with surface oxygen into formate species. When the catalyst was exposed to the combination of HCHO, O_2 and H_2O, besides the bands due to formate species, bands ascribed to dioxymethylene (1442 cm^{-1}), adsorbed water (1648 cm^{-1}) and hydroxyl groups (3240 cm^{-1}) were also detected. In addition, gas phase CO_2 (2360 cm^{-1}) was observed, which is in accordance with the observation that Au/CeO_2 (DPU) is active for HCHO oxidation at room temperature [51]. Comparing the reaction intermediates formed over the Au/CeO_2 (DPU) catalyst upon exposure to the different HCHO-containing streams, it is clear that formate species formed even in the absence of O_2 and H_2O, suggesting that the surface oxygen of the catalyst is active in the partial oxidation of HCHO into $[HCOO^-]_s$. The presence of both O_2 and H_2O in the feed gas similarly leads to the formation of formate species. The promoting effect of H_2O on deeper oxidation of the formate will be discussed below (Section 3.3.2).

By integrating the area of the formate $\nu_{as}(COO)$ band at 1575 cm^{-1} formed in the different HCHO-containing streams, the average rate of formate formation in the 60 min test was calculated for the Au/CeO_2 (DPN) and Au/CeO_2 (DPU) catalysts; the results are shown in Table 3. It is observed that the rate is the same in the absence or the presence of O_2 over Au/CeO_2 (DPN), suggesting that the presence of gas phase oxygen has no effect on formate formation. However, the rate is enhanced in the presence of H_2O and in the presence of both O_2 and H_2O, which implies that water promotes the formation of formate. This is not the case for Au/CeO_2 (DPU) for which the rate of formate formation is fastest in the 80 ppm $HCHO/N_2$ gas stream. Evidently, the adsorbed HCHO is rapidly oxidized into formate by the surface oxygen. In the presence of O_2 or H_2O the apparent rate is slower, in contrast to the results

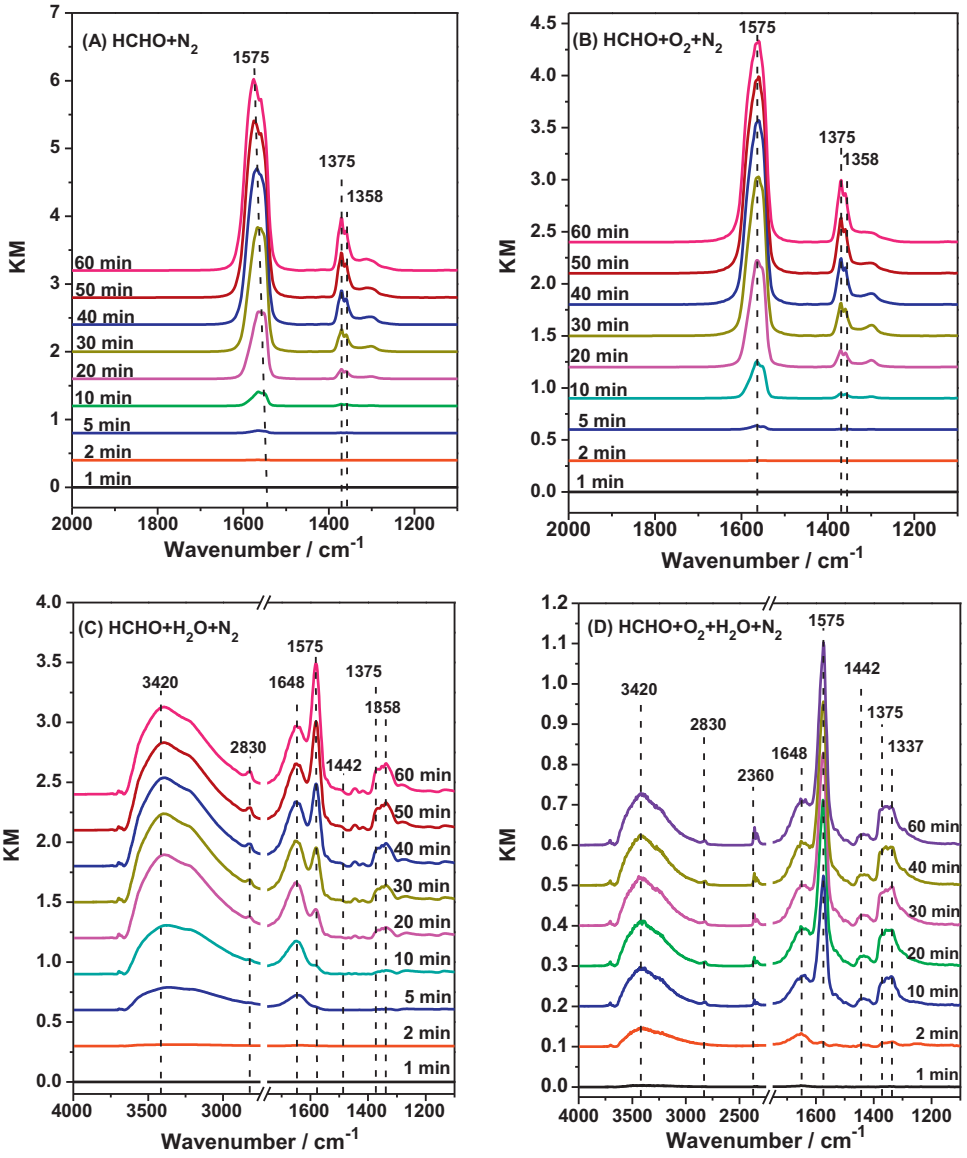

Fig. 9. *In situ* DRIFT spectra of HCHO adsorption on 1 wt% Au/CeO_2 (DPU) in different atmospheres at RT.

observed for the Au/CeO_2 (DPN) catalyst. Given that Au/CeO_2 (DPU) is very active even at room temperature, it is reasonable to believe that the slower rate of formate accumulation is due to its further oxidation. Noteworthy is the fact that the formate accumulation rate is slowest in the presence of both O_2 and H_2O, implying that the synergy of oxygen and water accelerates further oxidation of the formate.

Variations of the peak intensity of the intermediates with time on stream are compared for dry and wet air over the Au/CeO_2 (DPU) catalyst in Fig. 10A and B. Upon exposure to HCHO in dry air, bands due to formate species were observed. With increasing time, the band intensities increased and reached a constant value after 180 min. In comparison, in wet air the time required to reach constant formate band intensity was only 120 min. The variation of the measured peak area (1575 cm^{-1}, due to $\nu_{as}(COO)$) as a function of time is shown in Fig. 10C, which confirms that the peak area reached a constant value after 180 min on stream in dry air, as compared to only 120 min in wet air. Correlating this finding with the activity measurements (Fig. 5), it is apparent that the time required for formate formation exactly coincides with the induction period. This was further confirmed by the fact that the induction period is shortened at elevated reaction

Table 3
Rate of formate formation on 1 wt% Au/CeO_2 (DPN) and Au/CeO_2 (DPU) catalysts under different atmospheres.

Rate[a]	Atmosphere			
	80 ppm HCHO/N_2	80 ppm HCHO/21%O_2/N_2	80 ppm HCHO/H_2O(RH = 50%)/N_2	80 ppm HCHO/21%O_2/H_2O(RH = 50%)/N_2
Au/CeO_2 (DPN)	1.638	1.638	2.328	2.347
Au/CeO_2 (DPU)	2.211	1.788	0.921	0.352

[a] [The forming rate of formate species can be determined based on the kinetic dependence of intensity of the band due to formate. The rate was defined as Rate = $d[Area]/dt$ (*Area*: refers to the peak area of the band at 1575 cm^{-1} attributed to $\nu_{as}(COO)$ of formate; *t*: refers to the reaction time of 60 min)].

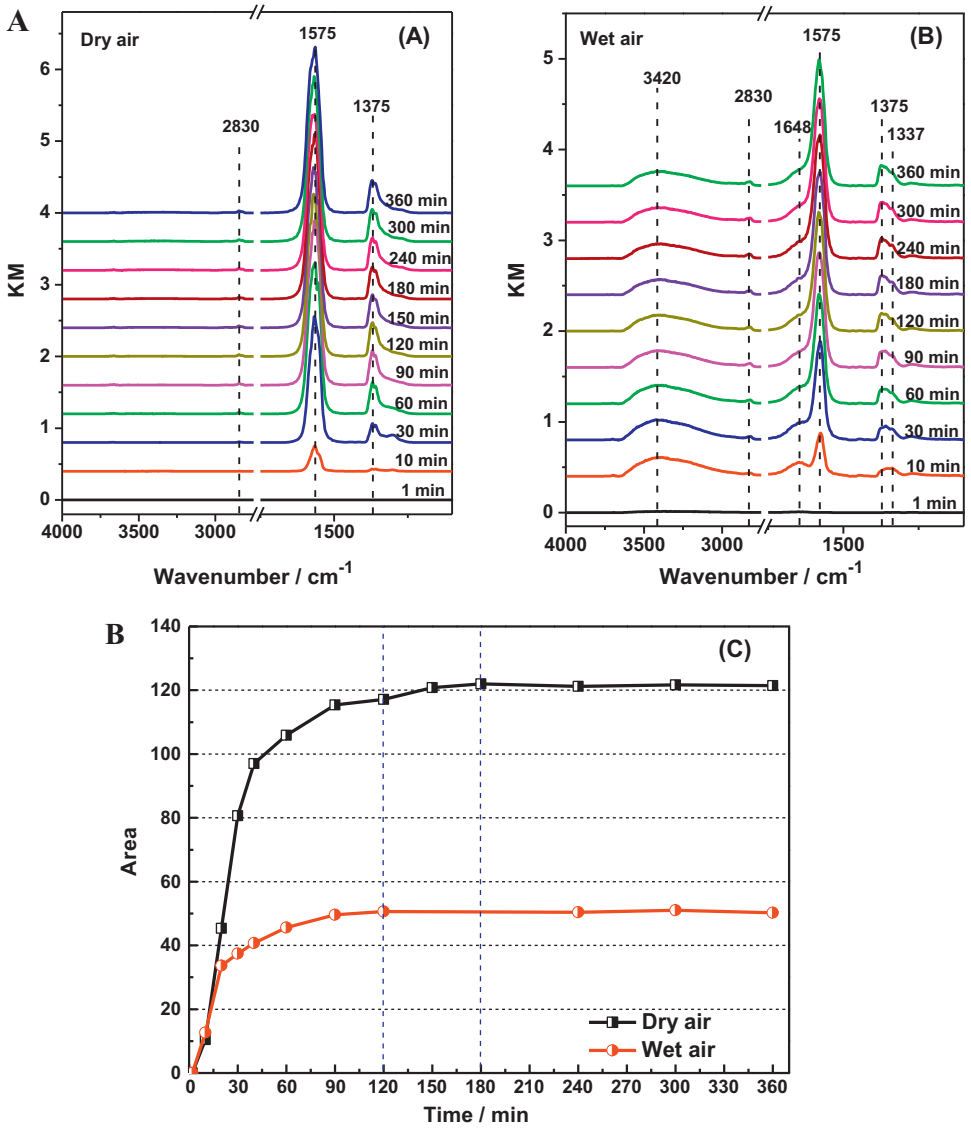

Fig. 10. (A) *In situ* DRIFT spectra of HCHO adsorption on 1 wt% Au/CeO_2 (DPU) in dry air; (B) *in situ* DRIFT spectra of HCHO adsorption on 1 wt% Au/CeO_2 (DPU) in wet air; (C) time dependence of the integrated area of the band at 1575 cm^{-1}.

temperature (see supporting information). These results suggest that the induction period is directly related to the formation of the reaction intermediates.

3.3.2. Consumption of reaction intermediates

The consumption of the formates upon their exposure to different gas streams was monitored by *in situ* DRIFTS, as shown in Fig. 11. The Au/CeO_2 (DPU) catalyst was first exposed to 80 ppm HCHO/21% O_2/H_2O (RH = 50%)/N_2 at room temperature for 60 min, followed by exposure to N_2, 21% O_2/N_2 or 21% O_2/H_2O (RH = 50%)/N_2 for 60 min. Compared to the spectra recorded after 60 min adsorption, the band due to formate species (1575 cm^{-1}) decreased in intensity upon the switch. The sharpest decrease was observed in the 21% O_2/H_2O (RH = 50%)/N_2 atmosphere, implying that the rate of formate consumption is fastest in the presence of 21% O_2/H_2O (RH = 50%)/N_2. The measured rates of formate disappearance are given in Table 4. According to these data, formate disappearance was the fastest in the 21% O_2/H_2O (RH = 50%)/N_2 gas stream, was moderate in the 21% O_2/N_2 gas stream and was the slowest in N_2. Therefore, it can be concluded that the presence of oxygen facilitated further oxidation of the formate.

In another experiment, after exposure to flowing feed gas containing 80 ppm HCHO/21% O_2/H_2O (RH = 50%)/N_2 for 60 min (Figs. 8D and 9D), the HCHO was switched off and *in situ* DRIFT spectra were recorded under a stream of 21% O_2/H_2O (RH = 50%)/N_2 (see Fig. 12). In the case of the Au/CeO_2 (DPN) catalyst, no obvious decrease in formate band intensity was observed upon exposure to the gas for 60 min at 25 °C and at 50 °C. However, upon heating to 100 °C, the intensities of the bands at 1575, 1550 and 1376 cm^{-1} decreased sharply, and complete oxidation of formate species occurred at 150 °C over the Au/CeO_2 (DPN) catalyst. In contrast, on standing at 25 °C for 60 min, the intensity of the band at

Table 4
Rate of formate consumption on 1 wt% Au/CeO_2 (DPU) under different atmospheres.

Atmosphere	21%O_2/H_2O(RH = 50%)/N_2	21%O_2/N_2	N_2
Rate[a]	0.173	0.134	0.097

[a] [The consuming rate of formate species can be determined based on the kinetic dependence of intensity of the band due to formate. The rate was defined as Rate = $d[Area]/dt$ (*Area*: refers to the peak area of the band at 1575 cm^{-1} attributed to ν_{as}(COO) of formate; *t*: refers to the reaction time of 60 min)].

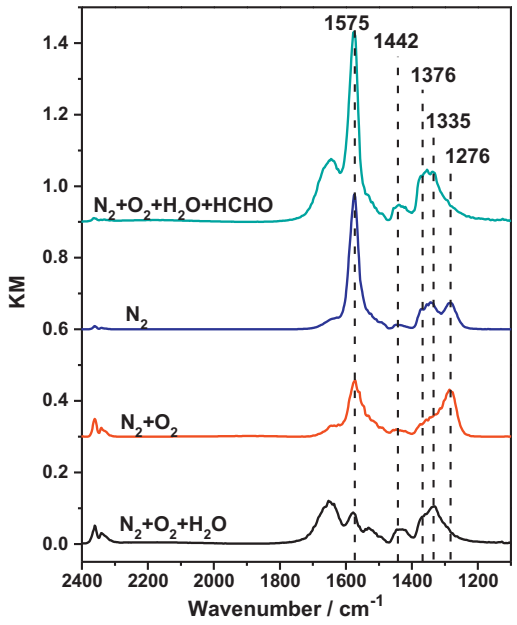

Fig. 11. *In situ* DRIFT spectra showing formate consumption on Au/CeO_2 (DPU) under different atmospheres following exposure to 80 ppm $HCHO/21\%O_2/H_2O$ (RH = 50%)/N_2 for 60 min.

1575 cm^{-1} decreased sharply over the Au/CeO_2 (DPU) catalyst. The intensity of the bands at 1537, 1442, 1376 and 1335 decreased weakly, which may be owing to the formate incomplete oxidation into carbonates [52]. These results confirm that formate species could be oxidized over the Au/CeO_2 (DPU) catalyst at room temperature, while formate oxidation requires elevated temperatures over the Au/CeO_2 (DPN) catalyst.

4. Discussion

Catalytic oxidation of HCHO at room temperature has been reported over several noble metal catalysts, such as Pt/TiO_2, Pt/Fe_2O_3 and Pt/MnO_x–CeO_2 [13–15]. To the best of our knowledge, there have been no reports concerning the total oxidation of HCHO over Au/CeO_2 catalysts at room temperature. Herein, two kinds of Au/CeO_2 catalyst prepared by the DP method, using urea and NaOH as precipitants, were investigated as catalysts for HCHO oxidation. The Au/CeO_2 (DPU) catalyst shows 100% conversion of HCHO into CO_2 in wet air at room temperature, even at the high GHSV of 143,000 h^{-1}, and the conversion is stable for at least 60 h. These results indicate that Au/CeO_2 (DPU) is a promising catalyst for indoor HCHO removal.

HRTEM, H_2-TPR and XPS techniques were used to characterize the physicochemical properties of the Au/CeO_2 samples. HRTEM results indicated that the mean Au particles size of Au/CeO_2 (DPU) catalyst was smaller than that of Au/CeO_2 (DPN) catalyst. The redox properties of ceria were greatly modified after loading with Au. The reduction temperature of the surface oxygen species was lowered to 100–200 °C, which is in line with previous reports concerning the generation of surface active oxygen species on CeO_2 resulting from its loading with metals such as Pt, Ag and Ni [21]. In fact, strong metal-support interactions (SMSI) have long been recognized; the effect of the support on catalytic performance is thought to originate from the influence of the support on the shape and size of the metal particles, from charge transfer from or to the metal nanoparticles, and/or from stabilization of ionic metal species. Fu et al. have proposed that the interaction of Au ions or atoms with ceria weakens the Ce—O bond, leading to the activation of the surface oxygen [53,54]. This proposal is supported by both DFT calculations and experimental data [55–57]. On the other hand, the results of experiments suggest that Au can adsorb on O sites, this adsorption being accompanied by a charge transfer process, which results in oxidation of the metal atom and reduction of the neighboring Ce^{4+} ion [53,58]. Indeed, evidence for such charge transfer is provided in this work by XPS measurements (Fig. 3). Ionic Au^{3+} and reduced Ce^{3+} species are present in both Au/CeO_2 samples, a higher amount of each being present in the Au/CeO_2 (DPU) catalyst. This confirms the presence of a strong metal interaction with the support. Indeed, the charge transfer from Au to CeO_2 weakened the Ce—O bond, leading to easier reduction of the CeO_2 surface oxygen. Comparing the two Au catalysts prepared using urea and NaOH as precipitants, higher concentrations of Au^{3+} and Ce^{3+} species in the Au/CeO_2 (DPU) catalyst with smaller mean Au particle sizes indicate a stronger interaction between Au and CeO_2 than in Au/CeO_2 (DPN), thereby facilitating the generation of comparatively more active surface

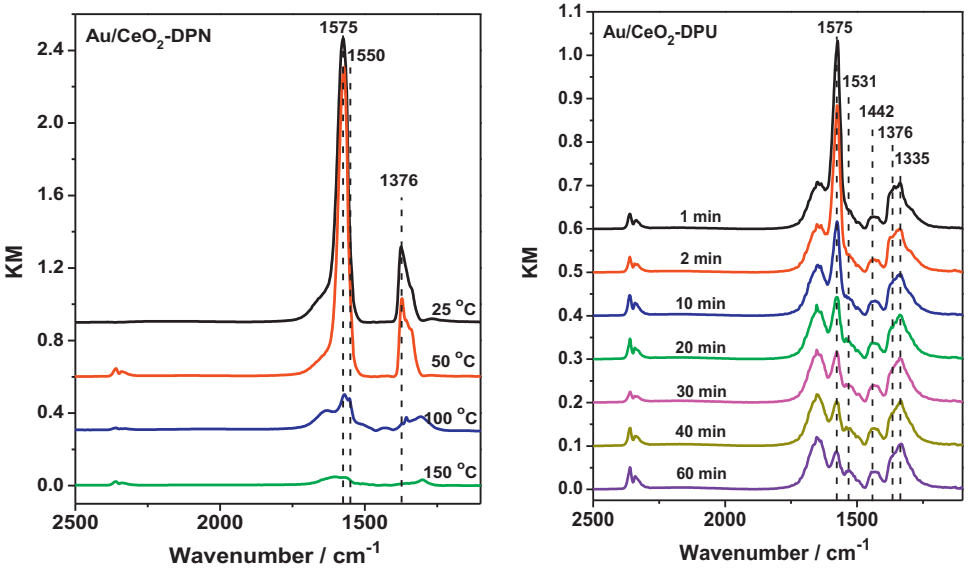

Fig. 12. *In situ* DRIFT spectra showing formate consumption on 1 wt% Au/CeO_2 (DPN) and 1 wt% Au/CeO_2 (DPU) catalysts in $21\%O_2/H_2O$ (RH = 50%)/N_2 following exposure of the catalysts to 80 ppm $HCHO/21\%O_2/H_2O$ (RH = 50%)/N_2 for 60 min.

oxygen species. These oxygen species could be reduced at low temperatures as evidenced by H_2-TPR (Fig. 2), which contributes to the superior activity of the Au/CeO_2 (DPU) catalyst for catalytic HCHO oxidation.

The formation and consumption of reaction intermediates were investigated using *in situ* DRIFTS. First, the influence of O_2 and H_2O on the formation of the intermediates was studied as shown in Figs. 8 and 9. It is apparent that HCHO could be rapidly oxidized into formate species in the absence of O_2 and/or H_2O in the feed over the Au/CeO_2 (DPN) catalyst (shown in Fig. 8A), suggesting that the adsorbed HCHO could be oxidized by the surface oxygen of the catalyst to formate [59]. This process can be described as follows:

$$HCHO(ad) + [O]_s \xrightarrow{k_1} [HCOO^-]_s + [\,]_s + H^+ \quad (1)$$

The presence of O_2 in the feed was found to have no effect on the rate of formate formation, implying that gas phase O_2 is not involved in formate generation, and that the formate was not further oxidized at room temperature over the Au/CeO_2 (DPN) catalyst [59,60]. However, when both H_2O and O_2 were present, the intensity of the bands ascribed to formate species was increased and the rate of formate appearance was faster than when H_2O was absent, which suggests that the presence of water accelerated the partial oxidation of HCHO to formate. This positive effect of H_2O has been reported previously [61,62]; it is postulated that introduction of water into the feed gas generates hydroxyl groups on the catalyst surface, and that these groups can adsorb the reactant and then oxidize it [62,63]. Following on from these reports, we propose the promoting effect of H_2O on HCHO partial oxidation can be expressed as follows:

$$HCHO(ad) + [OH]_s \xrightarrow{k'_1} [HCOO^-]_s + H^+ \quad (2)$$

As shown in Fig. 8C and D, the rate of formate appearance is similar in the presence of H_2O and H_2O/O_2, which again proves that gas phase O_2 is not required for partial oxidation of HCHO to formate.

Compared with the Au/CeO_2 (DPN) catalyst, the rate of formate formation over the Au/CeO_2 (DPU) catalyst was slower in the presence of O_2 and/or H_2O. As proved by the activity test (shown in Fig. 4), HCHO could be completely oxidized over the Au/CeO_2 (DPU) catalyst at room temperature, while no HCHO conversion was observed over the Au/CeO_2 (DPN) catalyst. This result suggests that formate could be further oxidized at room temperature according to Eqs. (3) and (4), which results in the slow rate of formate accumulation on the Au/CeO_2 (DPU) catalyst [46,64].

$$[HCOO^-]_s + [O]_s + H^+ \xrightarrow{k_2} CO_2 + H_2O + 2[\,] \quad (3)$$

$$[HCOO^-]_s + [OH] \xrightarrow{k'_2} CO_2 + H_2O \quad (4)$$

In addition, formate formation correlated with the induction period, as shown in Fig. 10 and Fig. S2. As evidenced by activity measurements, the induction period was shortened by the presence of H_2O and at higher temperatures, as shown in Fig. 5 and Fig. S1. It is the same case for the band intensities of the formate (1575 cm^{-1}) variation with time. Moreover, the time required for formate formation exactly coincided with the length of the induction period, while factors such as presence of H_2O in the feed gas or higher reaction temperatures, which enhanced the formate formation rate, shortened the induction period. Therefore, it is reasonable to conclude that the formation of formate reaction intermediates is the rate limiting step during the induction period.

DRIFTS results also provide insights into the effects of gas composition and temperature on the consumption of the formate intermediates. As shown in Fig. 11, the formates disappeared quickly in the presence of O_2 and H_2O, the rate of formate consumption being nearly twice that in pure nitrogen, which suggests that formate species were further oxidized to CO_2 and H_2O in the presence of O_2 and H_2O according to Eqs. (3) and (4). This is consistent with the finding that the rate of formate appearance was lowest in the presence of H_2O and O_2 at room temperature. In the presence of water, gas oxygen may be activated by water according to the equation ($O_2 + H_2O \rightarrow O^* + 2OH$), from this way the water could facilitate the activated of O_2 molecules. A similar phenomenon has also been reported over Au–TiO_2 catalyst [65].

It is obvious that though gas phase O_2 is not required for partial oxidation of HCHO to formates, the complete oxidation of them into CO_2 and H_2O need the participation of gas oxygen, as evidenced by comparison between the intermediates' consumption in N_2 and 21% O_2/N_2 gas stream as shown in Fig. 11, faster rate of consumption in the 21% O_2/N_2 gas stream were observed. The results clearly demonstrate the crucial role of oxygen in complete oxidation of the formates into CO_2 and H_2O.

The role of Au in activation of gas oxygen could be further evidenced by comparison the catalytic behaviors of CeO_2 and Au/CeO_2. As shown in Fig. S3, it is obvious that the partially oxidation of HCHO into formate (1578, 1376 and 1337 cm^{-1} which were due to the asymmetric ν_{as}(COO) stretch and symmetric ν_s(COO) stretch of formate, respectively) could occur on pure CeO_2 catalyst. However, no consumption of the formates was observed at room temperature and the formates oxidation requires elevated temperatures over the CeO_2 catalyst. In the case of the Au/CeO_2 (DPU) catalyst (shown in Fig. 12), the formate species (1575 and 1376 cm^{-1}) could be oxidized at room temperature. These results confirmed the role of Au in activation of oxygen for complete oxidation of the intermediates into CO_2 and H_2O, as illustrated in graphic abstract.

There was no consumption of formate at room temperature or at 50 °C over Au/CeO_2 (DPN), although upon increasing the temperature to 100 °C the bands ascribed to formate species decreased sharply, implying that formate was oxidized to CO_2 and H_2O. At 150 °C formate species were completely oxidized over Au/CeO_2 (DPN). However, the consumption of formate species occurred at room temperature over Au/CeO_2 (DPU). Significantly, the temperature required for complete formate consumption is consistent with the HCHO conversions shown in Fig. 4. Complete consumption of the formates was observed by DRIFTS at 150 °C over Au/CeO_2 (DPN), while at the same temperature 100% HCHO conversion was achieved. In comparison, Au/CeO_2 (DPU) is active at room temperature for HCHO oxidation, and the consumption of formate is also observed at room temperature by DRIFTS. From the above results, it is clear that although formate intermediates could form at room temperature over both of the catalysts, the activity for total oxidation of the formates to CO_2 and H_2O differs over the catalysts. Over Au/CeO_2 (DPU) catalyst, the oxidation of the intermediates occurs at room temperature and thus, it shows catalytic HCHO oxidation activity even at room temperature. Over Au/CeO_2 (DPN), higher temperatures are needed for the further oxidation of the formates. This implies that oxidation of the formate intermediates is the rate limiting step for catalytic oxidation of HCHO over Au/CeO_2 catalysts.

5. Conclusion

In this study it was found that Au/CeO_2 (DPU) afforded 100% conversion of HCHO into CO_2 in wet air at room temperature, even at high GHSV (143,000 h^{-1}). Moreover, the conversion was stable for at least 60 h. H_2-TPR and XPS analyses revealed that the interaction between Au and CeO_2 was stronger in Au/CeO_2 (DPU) than in the corresponding Au/CeO_2 (DPN) catalyst; we speculate that this stronger interaction resulted in increased amounts of active surface oxygen species and hence superior activity in HCHO oxidation.

In situ DRIFTS results suggested that the interaction of HCHO with surface oxygen resulted in the generation of $[HCOO^-]_s$, the rate limiting step for catalytic oxidation of HCHO over Au/CeO_2 being the oxidation of the formates to CO_2 and H_2O. Gas phase oxygen had no effect on the generation of $[HCOO^-]_s$, although it was necessary for total oxidation of $[HCOO^-]_s$ into CO_2 and H_2O. Water had a positive effect both on the formation and consumption of the formate reaction intermediates, leading to enhanced HCHO removal activity in wet air. This is significant for practical use, given that the presence of water is inevitable in air. Hence, Au/CeO_2 (DPU) is a promising catalyst for indoor HCHO removal.

Acknowledgments

The work was supported by the National Natural Foundation of China (Nos. 20573014 and 21073024), Natural Science Foundation of Liaoning Province (No. 201102034) and by the Program for New Century Excellent Talents in University (NCET-07-0136), as well as by the Fundamental Research Funds for the Central Universities (No. DUT12LK23).

Appendix A. Supplementary data

Supplementary data associated with this article can be found, in the online version, at http://dx.doi.org/10.1016/j.apcatb.2012.11.028.

References

[1] C. Chi Sing, L. Shun Cheng, L. Yok Sheung, H. Yu, Indoor and Built Environment 20 (2011) 420–429.
[2] M. Yan, W. Song, Z.-h. Chen, Carbon 49 (2011) 2869–2872.
[3] H. Nakayama, A. Hayashi, T. Eguchi, N. Nakamura, M. Tsuhako, Solid State Sciences 4 (2002) 1067–1070.
[4] Y. Wen, X. Tang, J. Li, J. Hao, L. Wei, X. Tang, Catalysis Communications 10 (2009) 1157–1160.
[5] W.J. Shen, X.F. Tang, Y.D. Xu, H.Q. Zhu, J.G. Wang, Applied Catalysis B 62 (2006) 265–273.
[6] S. Imamura, D. Uchihori, K. Utani, T. Ito, Catalysis Letters 24 (1994) 377–384.
[7] V. Lochař, Applied Catalysis A 309 (2006) 33–36.
[8] C. Shi, Y. Wang, A. Zhu, B. Chen, C. Au, Catalysis Communications 28 (2012) 18–22.
[9] C. Shi, B.-b. Chen, X.-s. Li, M. Crocker, Y. Wang, A.-M. Zhu, Chemical Engineering Journal 200–202 (2012) 729–737.
[10] J. Peng, S. Wang, Applied Catalysis B 73 (2007) 282–291.
[11] D.Y.C. Leung, H.B. Huang, ACS Catalysis 1 (2011) 348–354.
[12] H. He, C.B. Zhang, K. Tanaka, Applied Catalysis B 65 (2006) 37–43.
[13] D.Y.C. Leung, H.B. Huang, D.Q. Ye, Journal of Materials Chemistry 21 (2011) 9647–9652.
[14] M.J. Jia, N.H. An, Q.S. Yu, G. Liu, S.Y. Li, W.X. Zhang, Journal of Hazardous Materials 186 (2011) 1392–1397.
[15] W.J. Shen, X.F. Tang, J.L. Chen, X.M. Huang, Y. Xu, Applied Catalysis B 81 (2008) 115–121.
[16] M. Haruta, N. Yamada, T. Kobayashi, S. Iijima, Journal of Catalysis 115 (1989) 301–309.
[17] M.M. Wang, L. He, Y.M. Liu, Y. Cao, H.Y. He, K.N. Fan, Green Chemistry 13 (2011) 602–607.
[18] N. Yi, R. Si, H. Saltsburg, M. Flytzani-Stephanopoulos, Energy & Environmental Science 3 (2010) 831–837.
[19] M. Hosseini, T. Barakat, B.L. Su, G. De Weireld, S. Siffert, Applied Catalysis B 111 (2012) 218–224.
[20] M. Flytzani-Stephanopoulos, N. Yi, R. Si, H. Saltsburg, Applied Catalysis B 95 (2010) 87–92.
[21] L. Delannoy, K. Fajerwerg, C. Potvin, C. Methivier, C. Louis, Applied Catalysis B 94 (2010) 117–124.
[22] J.M. Rynkowski, I. Dobrosz-Gomez, I. Kocemba, Applied Catalysis B 83 (2008) 240–255.
[23] C.Y. Li, Y.N. Shen, R.S. Hu, P.P. Li, J. Zhang, Transactions of Nonferrous Metals Society of China 17 (2007) S1107–S1111.
[24] B.Q. Xu, Y.C. Hong, K.Q. Sun, K.H. Han, G. Liu, Catalysis Today 158 (2010) 415–422.
[25] M.L. Jia, H.F. Bai, Zhaorigetu, Y.N. Shen, Y.F. Li, Journal of Rare Earths 26 (2008) 528–531.
[26] H.Y. Zhu, Y.B. Zhang, S.S. Sheng, T. Wang, M.F. Adebajo, Journal of Molecular Catalysis A: Chemical 316 (2010) 100–105.
[27] J. Zhang, Y. Jin, C.Y. Li, Y.N. Shen, L. Han, Z.X. Hu, X.W. Di, Z.L. Liu, Applied Catalysis B 91 (2009) 11–20.
[28] B. Liu, Y. Liu, C. Li, W. Hu, P. Jing, Q. Wang, J. Zhang, Applied Catalysis B 1127 (2012) 47–58.
[29] H.-F. Li, N. Zhang, P. Chen, M.-F. Luo, J.-Q. Lu, Applied Catalysis B 110 (2011) 279–285.
[30] X. Chen, H.-Y. Zhu, J.-C. Zhao, Z.-F. Zheng, X.-P. Gao, Angewandte Chemie International Edition 47 (2008) 5353–5356.
[31] A.M. Zhu, D.Z. Zhao, X.S. Li, C. Shi, H.Y. Fan, Chemical Engineering Science 66 (2011) 3922–3929.
[32] A.M. Zhu, H.Y. Fan, C. Shi, X.S. Li, D.Z. Zhao, Y. Xu, Journal of Physics D: Applied Physics 42 (2009).
[33] Y. Wang, A. Zhu, Y. Zhang, C.T. Au, X. Yang, C. Shi, Applied Catalysis B 81 (2008) 141–149.
[34] S. Scire, S. Minico, C. Crisafulli, C. Satriano, A. Pistone, Applied Catalysis B 40 (2003) 43–49.
[35] C. Serre, F. Garin, G. Belot, G. Maire, Journal of Catalysis 141 (1993) 1–8.
[36] B. Liu, C. Li, Y. Zhang, Y. Liu, W. Hu, Q. Wang, L. Han, J. Zhang, Applied Catalysis B 111–112 (2012) 467–475.
[37] X.M. Shingo Watanabe, C. Song, Journal of Physical Chemistry C 113 (2009) 14249–14257.
[38] A.E. Aksoylu, B.S. Caglayan, Catalysis Communications 12 (2011) 1206–1211.
[39] H.Y. Kim, H.M. Lee, G. Henkelman, Journal of the American Chemical Society 134 (2012) 1560–1570.
[40] F. Esch, S. Fabris, L. Zhou, P. Fornasiero, G. Comelli, R. Rosei, Science 309 (2005) 752–755.
[41] N.J. Lawrence, J.R. Brewer, M.M. Ihrig, W.-N. Mei, C.L. Cheung, Nano Letters 11 (2011) 2666–2671.
[42] H.B. Huang, D.Y.C. Leung, Journal of Catalysis 280 (2011) 60–67.
[43] Z.P. Hao, C.Y. Ma, D.H. Wang, B.J. Dou, H.L. Wang, Environmental Science & Technology 45 (2011) 3628–3634.
[44] H.Y. Zhu, Y.N. Shen, Y.B. Zhang, L. Gao, M.L. Jia, Applied Catalysis B 79 (2008) 142–148.
[45] H.Y. Zhu, C.Y. Li, Y.N. Shen, M. Jia, S.S. Sheng, M.O. Adebajo, Catalysis Communications 9 (2008) 355–361.
[46] C. Zhang, F. Liu, K. Asakura, M. Flytzani-Stephanopoulos, H. He, Angewandte Chemie International Edition 51 (2012) 1–6.
[47] S.J. Park, I. Bae, I.-S. Nam, B.K. Cho, S.M. Jung, J.-H. Lee, Chemical Engineering Journal 195–196 (2012) 392–402.
[48] L. Wang, M. Sakurai, H. Kameyama, Journal of Hazardous Materials 167 (2009) 399–405.
[49] C. Li, K. Domen, K. Maruya, T. Onishi, Journal of Catalysis 125 (1990) 445–455.
[50] J. Bao, S. Sun, J.J. Ding, C. Gao, Z.M. Qi, C.X. Li, Catalysis Letters 137 (2010) 239–246.
[51] G. Busca, J. Lamotte, J.C. Lavalley, V. Lorenzelli, Journal of the American Chemical Society 109 (1987) 5197–5202.
[52] M. Schmal, L.G. Appel, J.G. Eon, Catalysis Letters 56 (1998) 199–202.
[53] Q. Fu, H. Saltsburg, M. Flytzani-Stephanopoulos, Science 301 (2003) 935–938.
[54] Y. Guan, D. Ligthart, Ö. Pirgon-Galin, J. Pieterse, R. van Santen, E. Hensen, Topics in Catalysis 54 (2011) 424–438.
[55] Z. Yang, B. He, Z. Lu, K. Hermansson, Journal of Physical Chemistry C 114 (2010) 4486–4494.
[56] Z.-P. Liu, S. Jenkins, D. King, Physical Review Letters 94 (2005).
[57] C. Zhang, A. Michaelides, D.A. King, S.J. Jenkins, Journal of the American Chemical Society 132 (2010) 2175–2182.
[58] Q. Fu, A. Weber, M. Flytzani-Stephanopoulos, Catalysis Letters 77 (2001) 87–95.
[59] Y.B. He, H.B. Ji, Chinese Journal of Catalysis 31 (2010) 171–175.
[60] C. Zhang, H. He, Catalysis Today 126 (2007) 345–350.
[61] M. Date, M. Okumura, S. Tsubota, M. Haruta, Angewandte Chemie International Edition 43 (2004) 2129–2132.
[62] H.H. Kung, M.C. Kung, C.K. Costello, Journal of Catalysis 216 (2003) 425–432.
[63] A. Luengnaruemitchai, D.T.K. Thoa, S. Osuwan, E. Gulari, International Journal of Hydrogen Energy 30 (2005) 981–987.
[64] J.S.Z. Jingjing Pei, HVAC&R Research 17 (2011) 476–503.
[65] Z. Zheng, J. Teo, X. Chen, Z. Zhong, H. Zhu, Chemistry: A European Journal 16 (2010) 1202–1211.